Hindawi
Computational and Mathematical Methods
Volume 2023, Article ID 9326843, 12 pages
https://doi.org/10.1155/2023/9326843

Research Article

Mathematical Modeling of COVID-19 with Periodic Transmission: The Case of South Africa

Belthasara Assan and Farai Nyabadza

Department of Mathematics and Applied Mathematics, University of Johannesburg, University Road and Kingsway Road, Auckland Park 2006, South Africa

Correspondence should be addressed to Farai Nyabadza; fnyabadza@uj.ac.za

Received 7 July 2022; Revised 2 December 2022; Accepted 30 December 2022; Published 15 February 2023

Academic Editor: Qichun Zhang

The data on SARS-CoV-2 (COVID-19) in South Africa show seasonal transmission patterns to date, with the peaks having occurred in winter and summer since the outbreaks began. The transmission dynamics have mainly been driven by variations in environmental factors and virus evolution, and the two are at the center of driving the different waves of the disease. It is thus important to understand the role of seasonality in the transmission dynamics of COVID-19. In this paper, a compartmental model with a time-dependent transmission rate is formulated and the stabilities of the steady states analyzed. We note that if $R_0 < 1$, the disease-free equilibrium is globally asymptotically stable, and the disease completely dies out; and when $R_0 > 1$, the system admits a positive periodic solution, and the disease is uniformly or periodically persistent. The model is fitted to data on new cases in South Africa for the first four waves. The model results indicate the need to consider seasonality in the transmission dynamics of COVID-19 and its importance in modeling fluctuations in the data for new cases. The potential impact of seasonality in the transmission patterns of COVID-19 and the public health implications is discussed.

1. Introduction

COVID-19 is an infectious disease caused by severe acute respiratory syndrome coronavirus 2 (SARS-CoV-2). The disease was first identified in December 2019 in Wuhan, the capital of Hubei, China, and has spread globally, resulting in the ongoing 2020 pandemic outbreak according to Worldometer [1]. It has caused substantial mortality and a major strain on healthcare systems according to Li et al. [2] and WHO [3]. At the opposite extreme, many countries lack the testing and public health resources to mount similar responses to the COVID-19 pandemic, which could result in the unhindered spread and catastrophic outbreaks. The disease has spread globally, and the virus has affected over 500 million people and caused the death of more than 6 million people as of April 2022.

Pharmaceutical interventions available are vaccinations and antiviral medicines according to Bugos [4]. Nonpharmaceutical interventions such as social distancing, intensive testing, and isolation of cases according to Diagne et al. [5] have been the mainstay in the control and management of COVID-19 in many African countries. The COVID-19 vaccines primarily prevent the development of severe disease that leads to hospitalization but not necessarily infection. That means vaccines do not block people from transmitting the pathogen to others. As a result, social distancing has quickly become an important consideration in mathematical modeling according to Kissler et al. [6], Matrajt and Leung [7], and Tuite et al. [8]. Social distancing is maintaining a physical distance between people and reducing the number of times people come into close contact with each other. It usually involves keeping a certain distance from others (distances specified differ from country to country and can change with time) and avoiding gathering together in large groups according to Anderson et al. [9]. It minimizes the probability that an uninfected person will come into physical contact with an infected person, thus suppressing the disease transmission, resulting in fewer hospitalizations and deaths.

Studies done on social distancing show that the adoption of relaxed social distancing measures reduces the number of

infected cases but does not shorten the duration of the epidemic waves. Increasing social distancing could reduce the number of COVID-19 new cases by 30% according to Makanda [10]. Researchers believe that social distancing offers more advantages than drawbacks since it can serve as a nonpharmacological tool to reduce the disease's proliferation rate.

Data on COVID-19 cases have shown trends of seasonal variations. Environmental factors and other climatic factors are often seasonal and could significantly affect disease dynamics according to Keeling et al. [11] and London and Yorke [12]. Seasonal cycles are ubiquitous features of influenza and other respiratory viral infections, particularly in temperate climates according to Martinez [13]. Like any other respiratory viral infection, COVID-19 has been found to exhibit some form of seasonality according to Chowdhury et al. [14] and Cai et al. [15]. The outcome of the research according to Chowdhury et al. [14] and Cai et al. [15] suggests that transmissibility of the COVID-19 can be affected by several meteorological factors, such as temperature and humidity. These conditions are probably favorable for the survival of the virus in the transmission routes. Research done by Huang et al. [16] found that 60% of the confirmed cases of COVID-19 occurred in places where the air temperature ranged from 5°C to 15°C, with a peak in cases at 11.54°C. Moreover, approximately 73.8% of the confirmed cases were concentrated in regions with absolute humidity of 3 g/m^3 to 10 g/m^3. SARS-CoV-2, however, appears to be spreading toward higher latitudes.

Seasonal patterns expose the limitations of many recent COVID-19 models that do not incorporate seasonality. In this paper, we consider South Africa, with two main climate seasons in a year. And during these periods, there has always been a surge in infections. We, therefore, propose a COVID-19 model that incorporates periodicity in the disease transmission pathway. In this case, the incidence is subject to periodicity. We divided our population into five subpopulations: susceptible individuals $S(t)$, exposed individuals $E(t)$, asymptomatic individuals $I_a(t)$, symptomatic individuals $I_s(t)$, and recovered individuals $R(t)$. We came up with a transmission rate $\beta(t)$, by incorporating the social distance parameter m in the transmission rate. We defined m to be periodically making our transmission rate periodic. We analyze the basic reproduction number, R_0 (using the next infection operator), and establish that R_0 is a sharp threshold for the COVID-19 models with periodic transmission. The method of analysis for extinction and persistence results for periodic epidemic systems is inspired by the research done by Bai and Zhou [17, 18]. We fitted our mathematical model to data obtained from the National Institute for Communicable Diseases [19] for the estimation of parameters and then simulated the efficacy of the social distance parameter.

This paper is organized as follows. In Section 2, we propose a new model for COVID-19 with periodic social distance parameters in the force of infection. A qualitative analysis of the model is investigated in Section 3. The usefulness of our model is then illustrated in Section 4 where we fit our model to the incidence data from South Africa. We conclude and discuss the paper in Section 5.

Table 1: Description of parameters used in the model.

Parameter	Description
Λ	Recruitment rate of humans.
μ	Natural mortality rate for humans.
$\delta(t, I_a, I_s)$	The disease transmission rate for humans, which is dependent on time.
κ	Progression rate of exposed individuals to the asymptomatic and symptomatic individuals.
γ_a, γ_s	Rate of recovery for asymptomatic and symptomatic individuals, respectively.
α	Rate of transfer from asymptomatic to symptomatic individuals.
ψ	Disease induce death rate.
$m(t)$	The periodic rate at which individuals distance themselves from each other.
η	Relative infectivity parameter for the symptomatic compared to the asymptomatic individuals.

2. The Mathematical Model

2.1. Model Formulation. We consider the total human population at the time t defined by $N(t)$. The total population is divided into five subpopulations, the susceptible individuals $S(t)$; the exposed individuals $E(t)$, those who are exposed to the virus but not diagnosed positive for COVID-19 yet; the asymptomatic individuals $I_a(t)$, those who are confirmed COVID-19 positive patients and do not have clinical symptoms; the symptomatic individuals $I_s(t)$, those who are confirmed COVID-19 positive patients and have clinical symptoms; and recovered individuals $R(t)$. Total population

$$N(t) = S(t) + E(t) + I_a(t) + I_s(t) + R(t). \tag{1}$$

The following compartmental diagram shows the flow of population between subpopulations.

Table 1 shows the parameter used in formulating the model.

From the compartmental model in Figure 1 and the described parameters in Table 1, the following nonautonomous dynamical system is derived to describe the dynamics of the transmission of COVID-19 with periodic social distancing in the force of infection:

$$\left.\begin{aligned}
\frac{dS}{dt} &= \Lambda - \delta(t, I_a, I_s)S - \mu S,\\
\frac{dE}{dt} &= \delta(t, I_a, I_s)S - (\mu + \kappa)E,\\
\frac{dI_a}{dt} &= \kappa p E - (\mu + \alpha + \gamma_a)I_a,\\
\frac{dI_s}{dt} &= \kappa(1-p)E + \alpha I_a - (\mu + \psi + \gamma_s)I_s,\\
\frac{dR}{dt} &= \gamma_s I_s + \gamma_a I_a - \mu R,
\end{aligned}\right\}, \tag{2}$$

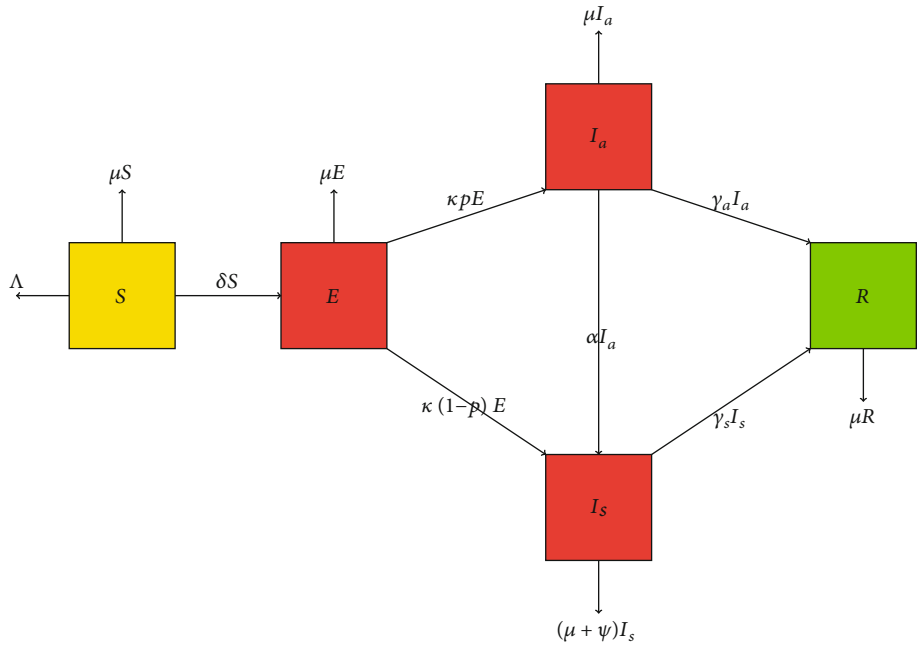

Figure 1: A compartmental model of COVID-19 with periodic transmission. The model consists of five subpopulations: susceptible $S(t)$, exposed $E(t)$, asymptomatic $I_a(t)$, symptomatic $I_s(t)$, and recovered $R(t)$. Solid arrows indicate movements among compartments.

where

$$\delta(t, I_a, I_s) = \beta(1 - m(t))\left(\frac{I_a + \eta I_s}{N}\right). \tag{3}$$

The incidence function $\delta(t, I_a, I_s)$ determines the rate at which new cases of COVID-19 are generated. The parameter η measures the difference in infectivity between I_a and I_s. The rates $m(t)$ are a periodic function of time with a common period, $\omega = 365/2 = 182.5$ days. Periodic transmission is often assumed to be sinusoidal, such that

$$m(t) = \hat{m}\left[1 + \bar{m}\sin\left(\frac{2\pi t}{182.5}\right)\right]. \tag{4}$$

The product $\hat{m}\bar{m}$ is the amplitude of the periodic oscillations in $m(t)$. There are no periodic infections when $\bar{m} = 0$. Here, $\hat{m}$ is thus the baseline value or the time-average value of social distancing.

3. Assumptions, Equilibrium Points, and Analysis

The function $\delta(t, I_a, I_s)$ is differential and periodic in time with period ω. That is,

$$\delta(t + \omega, I_a, I_s) = \delta(t, I_a, I_s). \tag{5}$$

To make biological sense, we assume that the function δ satisfies the following three conditions $(A1 - A3)$ for all $t \geq 0$:

$$A1 \quad \delta(t, 0, 0) = 0. \tag{6}$$

Setting all the derivatives of the dynamical system to zeros and setting all infected classes to be zero, that is, $(E, I_a, I_s) = (0, 0, 0)$, gives the disease-free equilibrium

$$E^0 = (S, E, I_a, I_s, R) = \left(\frac{\Lambda}{\mu}, 0, 0, 0, 0\right). \tag{7}$$

Assumption $(A1)$ ensures that the model has a unique and constant E^0.

$$A2 \quad \delta(t, I_a, I_s) \geq 0. \tag{8}$$

Assumption $A2$ ensures a nonnegative force of infection. So $\beta(1 - m(t))((I_a + \eta I_s)/N) \geq 0$ with the condition that $0 \leq m(t) \leq 1, \forall t > 0$.

$$A3 \quad \begin{aligned} \frac{\partial \delta(t, I_a, I_s)}{\partial I_a} &= \frac{\beta(1 - m(t))}{N} \geq 0, \\ \frac{\partial \delta(t, I_a, I_s)}{\partial I_s} &= \frac{\eta\beta(1 - m(t))}{N} \geq 0. \end{aligned} \tag{9}$$

Assumption $A3$ states that the rate of new infection increases with both the infected population size. Assumption $A4$ below shows that geometrically, the surface that represents the force of infection, δ, lies below its associated tangent plane at the origin. This means that the remainder term, R_1, from the truncated Taylor expansion of δ when the degree is equal to one is nonpositive. The second partial derivatives of the force of infection are

$A4\delta(t, I_a, I_s)$ is concave for any $t \geq 0$; i.e., the matrix

$$D^2\delta = \begin{bmatrix} \dfrac{\partial^2\delta}{\partial I_a^2} & \dfrac{\partial^2\delta}{\partial I_s \partial I_a} \\ \dfrac{\partial^2\delta}{\partial I_a \partial I_s} & \dfrac{\partial^2\delta}{\partial I_s^2} \end{bmatrix}, \tag{10}$$

is negative semidefinite everywhere. Since

$$A = \begin{bmatrix} I_a & I_s \end{bmatrix} \begin{bmatrix} \dfrac{\partial^2\delta}{\partial I_a^2} & \dfrac{\partial^2\delta}{\partial I_s \partial I_a} \\ \dfrac{\partial^2\delta}{\partial I_a \partial I_s} & \dfrac{\partial^2\delta}{\partial I_s^2} \end{bmatrix} \begin{bmatrix} I_a \\ I_s \end{bmatrix} \leq 0, \tag{11}$$

we have

$$R_1 \leq 0. \tag{12}$$

It follows that if $R_1 \leq 0$, the matrix A is negative semidefinite. The model shows that a single infected individual is sufficient for a positive infection rate.

3.1. The Basic Reproduction Number, Using the Next Infection Operator, L. Wang and Zhao [20] extended the framework in Diekmann et al. [21] to consider an epidemiological model in periodic environments. Let $\Phi_{-V(t)}$ and $\rho(\Phi_{-V(\omega)})$ be the monodromy matrix of the linear $\omega-$periodic system $dz/dt = -V(t)z$ and the spectral radius of $\Phi_{-V(\omega)}$, respectively. Assume $Y(t,s), t \geq s$ is the evolution operator of the linear $\omega-$periodic system

$$\frac{dy}{dt} = -V(t)y. \tag{13}$$

That is, for each $s \in \mathbb{R}$, the 3×3 matrix $Y(t,s)$ satisfies

$$\frac{dY(t,s)}{dt} = -V(t)Y(t,s), \forall t \geq s, Y(s,s) = I_{3\times 3}, \tag{14}$$

where $I_{3\times 3}$ is an identity matrix. In fluctuating environments, we assume that $\Phi(s)$ is the initial distribution of infectious individuals and is $\omega-$periodic in s. Then, $F(s)\Phi(s)$ is the rate of new infections produced by the infected individuals who were introduced at time s. Given that $t \geq s$, then, $Y(t,s)F(s)\Phi(s)$ gives the distribution of those infected individuals who were newly infected at time s and remain in the infected compartments at time t. It follows that

$$\lambda(t) \coloneqq \int_0^\infty Y(t-s)F(s)\phi(s)ds = \int_0^\infty Y(t,t-s)F(t-s)\phi(t-s)ds, \tag{15}$$

is the cumulative number of new infections at time t produced by all those infected individuals $\phi(s)$ introduced at the time previous to t. Let C_ω be the ordered Banach space of all $\omega-$periodic functions from $\mathbb{R}$ to $\mathbb{R}^3$, which is equipped with the maximum norm $\|.\|$ and the positive cone

$$C_\omega^+ \coloneqq \{\Phi \in C_\omega : \Phi(t) \geq 0, \forall t \in \mathbb{R}\}. \tag{16}$$

Then, we can define a linear operator $L : C_\omega \longrightarrow C_\omega$ by

$$L(\phi)(t) = \int_0^\infty Y(t,t-s)F(t-s)\phi(t-s)ds. \tag{17}$$

Here, L is the next infection operator, and we define the basic reproduction number as

$$R_0 \coloneqq \rho(L), \tag{18}$$

the spectral radius of L. We now define $F(t)$ and $V(t)$ according to equation (2).

$$F(t) = 0.9\begin{pmatrix} \delta S \\ 0 \\ 0 \end{pmatrix} = 0.9\begin{pmatrix} 0 & \dfrac{\beta(1-m(t))}{N}S & \dfrac{\eta\beta(1-m(t))}{N}S \\ 0 & 0 & 0 \\ 0 & 0 & 0 \end{pmatrix}. \tag{19}$$

Substituting $S = \Lambda/\mu$, we get

$$0.9F(t) = D_x F\left(t, E^0\right) = \begin{pmatrix} 0 & \dfrac{\beta(1-\widehat{m}[1+\bar{m}\sin(2\pi t/182.5)])\Lambda}{N\mu} & \dfrac{\eta\beta(1-\widehat{m}[1+\bar{m}\sin(2\pi t/182.5)])\Lambda}{N\mu} \\ 0 & 0 & 0 \\ 0 & 0 & 0 \end{pmatrix}, \tag{20}$$

$$V = 0.9\begin{pmatrix} (\mu+\kappa)E \\ -\kappa pE + (\mu+\alpha+\gamma_2)I_a \\ -\kappa(1-p)E - \alpha I_a + (\mu+\psi+\gamma_1)I_s \end{pmatrix} = \begin{pmatrix} U & 0 & 0 \\ -\kappa p & U_1 & 0 \\ -U_2 & -\alpha & U_3 \end{pmatrix}, \tag{21}$$

where

$$U = (\mu + \kappa),\ U_1 = (\mu + \alpha + \gamma_a),\ U_2 = \kappa(1-p) \text{ and } U_3 = (\mu + \psi + \gamma_s). \tag{22}$$

Also,

$$-V(t) = D_x V\left(t, E^0\right) = 1\begin{pmatrix} -U & 0 & 0 \\ \kappa p & -U_1 & 0 \\ U_2 & \alpha & -U_3 \end{pmatrix}. \tag{23}$$

$$\frac{dY(t,s)}{dt} = -V(t)Y(t,s), \forall t \geq s,\ Y(s,s) = I_{3\times 3}. \tag{24}$$

$$1\,Y(t,s) = \begin{pmatrix} e^{-U(t-s)} & 0 & 0 \\ \dfrac{\kappa p y_1}{U_1}\left(1 - e^{-U_1(t-s)}\right) & e^{-U_1(t-s)} & 0 \\ -Ce^{-U_2(t-s)} & C_1\left(1 - e^{-U_3(t-s)}\right) & e^{-U_3(t-s)} \end{pmatrix}, \tag{25}$$

where $C = -1/U_2(y_1 + \alpha y_4)$ and $C_1 = (\alpha/U_3)y_5$.

We numerically evaluate the next infection operator by

$$(L\phi)(t) = \int_0^{\infty} Y(t, t-s)F(t-s)\phi(t-s)ds = \int_0^{182.5} G(t,s)\phi(t-s)ds, \tag{26}$$

$$G(t,s) = \sum_{k=0}^{M} Y(t, t-s-k\omega)F(t-s-k\omega), \tag{27}$$

$$\approx N\sum_{k=0}^{M} 0.7\begin{pmatrix} 0 & \dfrac{\beta(1-\hat{m}[1+\bar{m}\sin(2\pi t/182.5)])\Lambda}{N\mu}e^{-U(t-s)} & \dfrac{\eta\beta(1-\hat{m}[1+\bar{m}\sin(2\pi t/182.5)])\Lambda}{N\mu}e^{-U(t-s)} \\ 0 & \dfrac{\kappa p y_1\beta(1-\hat{m}[1+\bar{m}\sin(2\pi t/182.5)])\Lambda}{N\mu U_1}\left(1-e^{-U_1^2(t-s)}\right) & \dfrac{\kappa p y_1\eta\beta(1-\hat{m}[1+\bar{m}\sin(2\pi t/182.5)])\Lambda}{N\mu\, U_1}\left(1-e^{-U_1^2(t-s)}\right) \\ 0 & \dfrac{\beta(1-\hat{m}[1+\bar{m}\sin(2\pi t/182.5)])\Lambda}{N\mu}Ce^{-U_2(t-s)} & \dfrac{\eta\beta(1-\hat{m}[1+\bar{m}\sin(2\pi t/182.5)])\Lambda}{N\mu}Ce^{-U_2(t-s)} \end{pmatrix}. \tag{28}$$

For some positive integer M

$$G(t,s) \approx \frac{\beta\Lambda}{\mu N}\sum_{k=0}^{M} 0.7\begin{pmatrix} 0 & \left(1-\hat{m}\left[1+\bar{m}\sin\left(\dfrac{2\pi(t-s)}{182.5}\right)\right]\right)e^{-U(s+k182.5)} & \eta\left(1-\hat{m}\left[1+\bar{m}\sin\left(\dfrac{2\pi(t-s)}{182.5}\right)\right]\right)e^{-U(s+k182.5)} \\ 0 & \kappa p y_1\left(1-\hat{m}\left[1+\bar{m}\sin\left(\dfrac{2\pi(t-s)}{182.5}\right)\right]\right)\left(1-e^{-U_1(s+k182.5)}\right) & \kappa p y_1\eta\left(1-\hat{m}\left[1+\bar{m}\sin\left(\dfrac{2\pi(t-s)}{182.5}\right)\right]\right)\left(1-e^{-U_1(s+k182.5)}\right) \\ 0 & \left(1-\hat{m}\left[1+\bar{m}\sin\left(\dfrac{2\pi(t-s)}{182.5}\right)\right]\right)Ce^{-U_2(s+k182.5)} & \eta\left(1-\hat{m}\left[1+\bar{m}\sin\left(\dfrac{2\pi(t-s)}{182.5}\right)\right]\right)Ce^{-U_2(s+k182.5)} \end{pmatrix}. \tag{29}$$

To compute the basic reproduction number R_0, we reduce the operator eigenvalue problem to a matrix eigenvalue problem in the form of $Ax = \lambda x$, where matrix A can be constructed by arranging the entries of the function G. The basic reproduction number R_0 can then be approximated by numerically calculating the spectral radius of the matrix A. The monodromy matrix of differential equation (14) is

$$\Phi_{-V(t)} = Y(t,0) = \begin{pmatrix} e^{-U(t)} & 0 & 0 \\ \dfrac{\kappa p y_1}{U_1}\left(1-e^{-(U_1(t)}\right) & e^{-U_1(t)} & 0 \\ Ce^{-U_2(t)} & C_1\left(1-e^{-U_3(t)}\right) & e^{-U_3(t)} \end{pmatrix}. \tag{30}$$

It follows that the eigenvalues of any lower triangular matrix are the diagonal elements.

Thus, the spectral radius of $\rho(\Phi_{V(182.5)}) = \max\{e^{-U(182.5)}, e^{-U_1(182.5)}, e^{-U_3(182.5)}\}$.

Lemma 1. *The following statements are valid for equation (2)*
$R_0 = 1$ *if and only if* $\rho(\Phi_{F-V}(\omega)) = 1$.
$R_0 > 1$ *if and only if* $\rho(\Phi_{F-V}(\omega)) > 1$.
$R_0 < 1$ *if and only if* $\rho(\Phi_{F-V}(\omega)) < 1$.

The disease free equilibrium, E^0, is locally asymptotically stable if $R_0 < 1$ and unstable if $R_0 > 1$.

Proof. Since model 1 satisfies conditions $(A1)$—$(A7)$ in Assan et al. [22], it follows that Theorem 2.2 of Wang and Zhao [20], hold for all conditions. □

3.2. Disease Extinction. In this subsection, we analyze the global stability of the disease-free equilibrium point for the system (2). These give conditions for disease extinction. Suppose we have the matrix function

$$F(t) - V(t) = \begin{pmatrix} -U & \dfrac{\beta(1-\hat{m}[1+\bar{m}\sin(2\pi t/182.5)])\Lambda}{N\mu} & \dfrac{\eta\beta(1-\hat{m}[1+\bar{m}\sin(2\pi t/182.5)])\Lambda}{N\mu} \\ \kappa p & -U_1 & 0 \\ U_2 & \alpha & -U_3 \end{pmatrix}, \tag{31}$$

where $F(t) = D\mathcal{F}(E^0)$ and $V(t) = D\mathcal{V}(E^0)$. The disease-free equilibrium E^0 is globally asymptotically stable if all the eigenvalues of the matrix $\mathrm{DE}^0 = \{F(t) - V(t)\}$ have positive real parts. The matrix function of equation (31) is irreducible, continuous, cooperative, and ω-periodic. Let $\Phi_{(F-V)}(t)$ be the fundamental solution matrix of the linear ordinary differential system:

$$z' = [F(t) - V(t)]z, \tag{32}$$

where $z = [E, I_a, I_s]^T$ and $\rho(\Phi_{F-V}(\omega))$ are the spectral radius of $(\Phi_{F-V}(\omega))$.

Lemma 2. *Let* $b = (1/\omega)\ln\rho(\Phi(F-V)(\omega)$. *Then, there exist a positive* ω*-periodic function* $v(t)$ *such that* $e^{bt}v(t)$ *is a solution to equation (32).*

Proof.

$$0.8\frac{d}{dt}\begin{bmatrix} E \\ I_a \\ I_s \end{bmatrix} = \begin{bmatrix} -U & \dfrac{\beta(1-\hat{m}[1+\bar{m}\sin(2\pi\, t/182.5)])\Lambda}{N\mu} & \dfrac{\eta\beta(1-\hat{m}[1+\bar{m}\sin(2\pi\, t/182.5)])\Lambda}{N\mu} \\ \kappa p & -U_1 & 0 \\ U_2 & \alpha & -U_3 \end{bmatrix}\begin{bmatrix} E \\ I_a \\ I_s \end{bmatrix}\begin{bmatrix} E \\ I_a \\ I_s \end{bmatrix} = e^{bt}v(t). \tag{33}$$

Since $R_0 < 1$; then, $\rho(\Phi_f(182.5)) < 1$, then $b < 0$, it follows that $R_0 < 1$ implies

$$\lim_{t\longrightarrow\infty} e^{bt}v(t) = [0,0,0]^T. \tag{34}$$

Considering and using $A4$, $R_1 \le 0$, this follows

$$\begin{aligned} \frac{\mathrm{d}}{\mathrm{dt}}\begin{bmatrix} E \\ I_a \\ I_s \end{bmatrix} = \begin{bmatrix} \delta(t, I_a, I_s)S - UE \\ \kappa pE - U_1 I_a \\ U_2 E + \alpha I_a - U_3 I_s \end{bmatrix}, &= \begin{bmatrix} -U & \dfrac{\beta(1-\hat{m}[1+\bar{m}\sin(2\pi t/182.5)])\Lambda}{N\mu} & \dfrac{\eta\beta(1-\hat{m}[1+\bar{m}\sin(2\pi t/182.5)])\Lambda}{N\mu} \\ \kappa p & -U_1 & 0 \\ U_2 & \alpha & -U_3 \end{bmatrix}\begin{bmatrix} E \\ I_a \\ I_s \end{bmatrix} + R_1, \\ &\le \begin{bmatrix} -U & \dfrac{\beta(1-\hat{m}[1+\bar{m}\sin(2\pi t/182.5)])\Lambda}{N\mu} & \dfrac{\eta\beta(1-\hat{m}[1+\bar{m}\sin(2\pi t/182.5)])\Lambda}{N\mu} \\ \kappa p & -U_1 & 0 \\ U_2 & \alpha & -U_3 \end{bmatrix}\begin{bmatrix} E \\ I_a \\ I_s \end{bmatrix}. \end{aligned} \tag{35}$$

From (Theorem 2.2 by Wang and Zhao [20]), $R_0 < 1$ if and only if $\rho(\Phi_{(F-V)}(182.5)) < 1$. Therefore, $b < 0$. It is clear that

$$\lim_{t\longrightarrow\infty} E(t) = 0, \lim_{t\longrightarrow\infty} I_a(t) = 0, \quad \text{and} \quad \lim_{t\longrightarrow\infty} I_s(t) = 0, \quad (36)$$

Next, we consider the last equation in equation (2). For any $\varepsilon > 0$, there exists $T > 0$ such whenever $t > T$, we have

$$I_a = \frac{\varepsilon_a}{\gamma_a}, I_s = \frac{\varepsilon_s}{\gamma_s} \quad \text{and} \quad \frac{\mathrm{dR}}{\mathrm{dt}} < \varepsilon_a + \varepsilon_s - \mu R. \quad (37)$$

$R(t) < \varepsilon_a + \varepsilon_s/\mu$ for $t > T$. Since $\varepsilon > 0$ is arbitrary so

$$\lim_{t\longrightarrow\infty} R(t) = 0. \quad (38)$$

Since the total population $N(t) = S(t) + E(t) + I_a(t) + I_s(t) + R(t)$, we have that

$$\lim_{t\longrightarrow\infty} S(t) = \frac{\Lambda}{\mu}. \quad (39)$$

We thus have the following result. □

Theorem 3. *If $R_0 < 1$, then the disease-free equilibrium of Equation of 1 is globally asymptotically stable.*

Theorem 3 shows that the disease will completely die out as long as $R_0 < 1$. This further implies that reducing and keeping R_0 below 1 would be sufficient to eradicate COVID-19 infection even with periodic transmission.

3.3. Disease Persistence. In this subsection, we consider the dynamics of equation (2) when $R_0 > 1$, where E^1 be the endemic equilibrium point for equation (2). Let us consider also the following set:

$$X \coloneqq \mathbb{R}^5_+, \quad (40)$$

$$X_0 \coloneqq \{(S, E, I_a, I_s, R) \in X | S > 0, E > 0, I_a > 0, I_s > 0, R > 0\}, \quad (41)$$

$$\partial X_0 \coloneqq X \setminus X_0. \quad (42)$$

Let $u(t, \phi)$ be the unique solution of equation (2) with initial condition ϕ, $\Phi(t)$ semiflow generated by periodic equation (2) and $P : X \longrightarrow X$ the Poincaré map associated with equation (2), namely,

$$P(\phi) = (\omega)\phi = u(\omega, \phi), \forall \phi \in X, \quad (43)$$

$$P^m(\phi) = (m\omega)\phi = u(m\omega, \phi), \forall m \geq 0. \quad (44)$$

Proposition 4. *The set X_0 and ∂X_0 are positively invariant under the flow induced by equation (2).*

Proof. For any initial condition $\psi \in X_0$, by solving equation (2), we derive and obtain

$$\begin{aligned}
S(t) &= \exp\left(-\int_0^t h(s)ds\right)\left[S(0) + \Lambda\int_0^t \exp\left(\int_0^s h(\tau)d\tau\right)ds\right],\\
&\geq \Lambda \exp\left(-\int_0^t h(s)ds\right)\left[\int_0^t \exp\left(\int_0^s h(\tau)d\tau\right)ds\right] > 0, \forall t > 0,\\
E(t) &= \exp(-Ut)\left(E(0) + \int_0^t \delta(s, I_a, I_s)S(s)\exp(Us)ds\right),\\
&\geq \exp(-Ut)\left(\int_0^t \delta(s, I_a, I_s)S(s)\exp(Us)ds\right) > 0, \forall t > 0,\\
I_a(t) &= \exp(-U_1 t)\left(I_a(0) + \int_0^t \kappa p E(s)\exp(U_1 s)ds\right),\\
&\geq \exp(-U_1 t)\left(\kappa p\int_0^t E(s)\exp(U_1 s)ds\right) > 0, \forall t > 0,\\
I_s(t) &= \exp(-U_3 t)\left(I_s(0) + \int_0^t U_2 E(s) + \alpha I_a(s)\exp(U_3 s)ds\right),\\
&\geq \exp(-U_3 t)\left(\int_0^t U_2 E(s) + \alpha I_a(s)\exp(U_3 s)ds\right) > 0, \forall t > 0,\\
R(t) &= \exp(-\mu t)\left(R(0) + \int_0^t (\gamma_s I_s(s) + \gamma_a I_a(s))\exp(\mu s)ds\right),\\
&\geq \exp(-\mu t)\left(\int_0^t (\gamma_s I_s(s) + \gamma_a I_a(s))\exp(\mu s)ds\right) > 0, \forall t > 0,
\end{aligned} \quad (45)$$

where $h = (\delta(t, I_a, I_s) - \mu)S$. □

Thus, X_0 is positively invariant. Since X is positively invariant and ∂X_0 is relatively closed in X, it yields that ∂X_0 is positively invariant.

The compact Ω is defined as a positive invariant set for the equation (2), which attracts all positive orbits in $\mathbb{R}^5_+$, and the solutions are bounded. Ω attracts all positive orbits in X, which implies that the discrete-time system $P : X \longrightarrow X$ is point dissipative. Moreover, $\forall n_0 \geq 1$, and P^{n_0} is compact, it then follows that P admits a global attractor in X.

Lemma 5. *If $R_0 > 1$,there exists $\eta > 0$ such that when $\|\phi - E^1\| \leq \eta$, $\forall \phi \in X_0$, we have*

$$\limsup_{n\longrightarrow\infty} \left\|P^n(\phi) - E^1\right\| \geq \eta. \quad (46)$$

Proof. Suppose by contradiction that $\limsup_{n\longrightarrow\infty} \|P^n(\phi) - E^1\| < \eta$ for some $\phi \in X_0$. Then, there exists an integer $N_1 \geq 1$ such that for all $n \geq N_1$, $\|P^n(\phi) - E^1\| < \eta$. By the continuity of the solution $u(t, \phi)$, we have $\|u(t, P^n(\phi)) - u(t, E^1) \leq \sigma\|$ for all $t \geq 0$ and $\sigma > 0$. For all $t \geq 0$, let $t = n\omega + t'$, where $t' \in [0, \omega]$ and $n = [t/\omega]$. $[t/\omega]$ is the greatest integer less or equal to t/ω. If $\|\phi - E^1\| \leq \eta$, then by the continuity of the solution $u(t, \phi)$, we have

$$\begin{aligned}\left\|u(t,\phi)-u\left(t,E^1\right)\right\| &= \left\|u\left(t'+n\omega,\phi\right)-u\left(t'+n\omega,E^1\right)\right\|,\\ &= \left\|u\left(t'+n\omega\right)\phi-\phi\left(t'+n\omega\right)E^1\right)\right\|,\\ &= \left\|\Phi\left(t'\right)\Phi(n\omega)\phi-\Phi\left(t'\right)\Phi(n\omega)E^1\right\|,\\ &= \left\|\Phi\left(t'\right)P^n(\Phi)-\Phi\left(t'\right)P^n\left(E^1\right)\right\|,\\ &= \left\|\Phi\left(t'\right)P^n(\Phi)-\Phi\left(t'\right)E^1\right\|\geq\sigma.\end{aligned} \tag{47}$$

Moreover, there exists $\sigma^*>0$ such that for all $t\in[0,\omega]$,

$$\frac{S(t)}{N}\geq\frac{S^*}{N^*}-\sigma^*. \tag{48}$$

□

Hence, we obtain the following equation:

$$\frac{\mathrm{dE}}{\mathrm{dt}}\geq\beta(1-m(t))(I_a+\eta I_s)\left(\frac{S^*}{N^*}-\sigma^*\right)-(\mu+\kappa)E, \tag{49}$$

$$\frac{\mathrm{dI_a}}{\mathrm{dt}}=\kappa pE-(\mu+\alpha+\gamma_a)I_a, \tag{50}$$

$$\frac{\mathrm{dI_s}}{\mathrm{dt}}=\kappa(1-p)E+\alpha I_a-(\mu+\psi+\gamma_s)I_s, \tag{51}$$

$$\frac{\mathrm{dR}}{\mathrm{dt}}=\gamma_s I_s+\gamma_a I_a-\mu R. \tag{52}$$

Let us consider the following auxiliary linear equation:

$$\frac{\mathrm{d}\bar{Z}(\mathrm{t})}{\mathrm{dt}}=M_{\sigma^*}(t)\bar{Z}(t), \tag{53}$$

where

$$\bar{Z}(t)=\left(\bar{E}(t),\bar{I}_a(t),\bar{I}_s(t),\bar{R}(t)\right)^T, \tag{54}$$

and $M_{\sigma^*}(t)$ a matrix defined by

$$\begin{pmatrix} U & \dfrac{\beta(1-m(t))}{N}q & \dfrac{\eta\beta(1-m(t))}{N}q & 0\\ \kappa p & U_1 & 0 & 0\\ U_2 & \alpha & U_3 & 0\\ 0 & \gamma_a & \gamma_s & -\mu \end{pmatrix}, \tag{55}$$

where $q=(S^*/N^*)-\sigma^*$.

By Lemma 2, there exists a positive $\omega-$periodic function $v(t)$ such that $\bar{Z}(t)=e^{rt}v(t)$ is a solution of equation (53) with $r=(1/\omega)\ln\rho(\Phi_{M\sigma^*}(\omega)).\rho(\Phi_{M\sigma^*}(\omega))>1$ implies that $r>0$. In this case, $\bar{Z}(t)\longrightarrow\infty$ as $t\longrightarrow\infty$. Applying the theorem of comparison of Lakshmikantham et al. [23], we have

$$\lim_{x\longrightarrow\infty}|(E(t),I_a(t),I_s(t),\mathrm{R}(t)|=\infty, \tag{56}$$

that contradicts the fact that solutions are bounded.

Theorem 6. *If $R_0>1$, there exists $\xi>0$ such that any solution $u(t,\varphi)$ with the initial condition $\phi\in X_0$ satisfies*

$$\liminf_{t\longrightarrow\infty}S(t)\geq\xi,\quad\liminf_{t\longrightarrow\infty}E(t)\geq\xi,\quad\liminf_{t\longrightarrow\infty}I_a(t)\geq\xi,\quad\liminf_{t\longrightarrow\infty}I_s(t)\geq\xi, \tag{57}$$

$$\liminf_{t\longrightarrow\infty}R(t)\geq\xi, \tag{58}$$

and equation (2) has at least one positive periodic solution.

Proof. Let us consider the following sets:

$$M_\partial=\{\phi\in\partial X_0:P^n(\phi)\in\partial X_0,n\geq0\}, \tag{59}$$

$$D=\{(S,0,0,0,0)\in X:S\geq0\}. \tag{60}$$

It is clear that $D\subset M_\partial$. So we must prove that $M_\partial\subset D$. That means, for any initial condition $\phi\in\partial X_0$,$E(n\omega)=0$ or $I_a(n\omega)=0$ or $I_s(n\omega)=0$ or $R(n\omega)=0$ or, for all $n\geq0$. Let $\phi\in\partial X_0$. Suppose by contradiction that there exists an integer $n_1\geq0$ such that $E(n_1\omega)>0$ or $I_a(n_1\omega)>0$ or $I_s(n_1\omega)>0$ or $R(n_1\omega)>0$. Then, by replacing the initial time $t=0$ by $t=n_1\omega$ in equations (45)–(53), we obtain $S(t)>0,E(t)>0,I_a(t)>0,I_s(t)>0,R(t)>0$ that contradicts the fact that ∂X_0 is positively invariant. The equality $M_\partial=D$ implies that E^1 is a fixed point of P and acyclic in M_∂, every solution in M_∂ approaches to E^1. Moreover, Lemma 5 implies that E^1 is an isolated invariant set in X and $W_s(E^1)\cap X_0=\varnothing$. By the acyclicity theorem on uniform persistence for maps (Zhao [24], Theorem 3.1.1), it then follows that P is uniformly persistent with respect to $(X_0,\partial X_0)$. So the periodic semiflow $\Phi(t)$ is also uniformly persistent. Hence, there exists $\xi>0$ such that

$$\liminf_{t\longrightarrow\infty}S(t)\geq\xi,\quad\liminf_{t\longrightarrow\infty}E(t)\geq\xi,\quad\liminf_{t\longrightarrow\infty}I_a(t)\geq\xi,\quad\liminf_{t\longrightarrow\infty}I_s(t)\geq\xi, \tag{61}$$

$$\liminf_{t\longrightarrow\infty}R(t)\geq\xi. \tag{62}$$

Furthermore, from (Zhao [24], Theorem 1.3.6), the system (2) has at least one periodic solution $u(t,\phi^*)$ with $\phi^*\in X_0$. Now, let us prove that $S^*(0)$ is positive. If $S^*(0)=0$; then, we obtain that $S^*(0)>0$ for all $t>0$. But using the periodicity of the solution, we have $S(0)=S(n\omega)=0$ which is also a contradiction. □

4. Numerical Simulations

We now apply our model to the COVID-19 pandemic in South Africa. We use the outbreak data published daily by the National Institute for Communicable Diseases [19]. These data sets contain the daily reported new cases, cumulative cases, and disease-induced deaths in South Africa, for

each province in South Africa. We, however, in this work considered the national data.

The numerical simulations were done using Python software. We use the force of infection with interventions, given by

$$\beta(1-m(t))\left(\frac{I_a+\eta I_s}{N}\right) \text{ where } m(t)=\hat{m}\left[1+\bar{m}\sin\left(\frac{2\pi t}{182.5}\right)\right]. \tag{63}$$

In our case where the intervention is social distancing, m, it is assumed to be periodic, due to the fluctuations in the existing data. The parameter β is positive and denotes the maximum value of the transmission rate. We conduct numerical simulations for an epidemic period starting from 27th of March 2020, when South Africa was locked and social distancing was observed in every place to 19th of April 2022. Our time was set in days and given our period-ω to be 182.5 days, due to the number of waves in a year. We fit the constructed model to new cases of South Africa DSFSI [25] to illustrate our mathematical results. The total population of South Africa in the year 2020 was 59.31 million Google [26]. The mortality rate μ was obtained by using the life expectancy of South Africa which was found to be 64.3 years. The transmission rate was obtained through data fitting and all other parameters that were used in this section. The social distancing parameter $m(t)$ and the proportion of exposed individuals p are all in the interval (0,1).

To estimate the values for the rest of the parameters not given above, we fit our model to the new cases reported daily in South Africa from 27th of March 2020 to 19th of April 2022. Studies reveal that the true number of COVID-19 infections in Africa could be 97% higher than the number of confirmed reported cases according to Schlein [27] and Kleynhans et al. [28]. The initial conditions of all state variables are taken from the data. We set our initial conditions for each wave as

$$\left.\begin{array}{ll}\text{Firstwave}: & E0=100, I_a0=96, I_s0=1, R0=0,\\ \text{Secondwave}: & E0=34000, I_a0=32903, I_s0=1240, R0=591208,\\ \text{Thirdwave}: & E0=16972, I_a0=16282, I_s0=438, R0=890429,\\ \text{Fourthwave}: & E0=16000, I_a0=15296, I_s0=598, R0=1331581.\end{array}\right\}. \tag{64}$$

Initial conditions for susceptible and the asymptotic infectives are given by $S0=N-(E0+I_a0+I_s0+R0)$ and $I_a0=(97/3)\times I_s0$, respectively.

Table 2 gives the start dates, end dates, and the number of days in which each wave occurs. We thus consider the system

$$\frac{dX_0}{dt}=f(X_0), \quad \text{for} \quad t=\begin{cases} t_0\le t<t_1,\\ t_1\le t<t_2,\\ t_2\le t<t_3,\\ t_3\le t<t_4,\end{cases} \tag{65}$$

where

Table 2: Time and days for the waves used in the estimation of initial conditions.

Waves	Start date	End date	Days
1	27th of March 2020	11th of September 2020	178
2	11th of September 2020	10th of April 2021	200
3	11th of April 2021	29th of October 2021	200
4	30th of October 2021	19th of April 2022	171

Table 3: Parameter estimation of COVID-19 in South Africa for the first four waves in days.

Estimated parameters	Wave 1	Wave 2	Wave 3	Wave 4
Λ	1.00×10^{4}	6.66×10^{6}	1.59×10^{7}	1.70×10^{7}
β	3.33×10^{-1}	2.49×10^{-1}	1.90×10^{-1}	2.1×10^{-1}
κ	3.00×10^{-2}	3.45×10^{-2}	4.90×10^{-2}	1.60×10^{-3}
γ_a	7.00×10^{-2}	1.33×10^{-4}	1.28×10^{-3}	3.90×10^{-2}
γ_s	3.33×10^{-2}	4.42×10^{-2}	5.10×10^{-1}	2.70×10^{-1}
α	1.43×10^{-1}	1.70×10^{-2}	9.00×10^{-3}	2.10×10^{-3}
ψ	1.43×10^{-1}	2.45×10^{-1}	9.90×10^{-3}	4.50×10^{-3}
η	1.60×10^{-2}	4.58×10^{-1}	1.07×10^{-1}	8.50×10^{-2}

$t_0=27^{\text{th}}$ of March 2020, $t_1=11^{\text{th}}$ of September 2020, $t_2=10^{\text{th}}$ of April 2021, $t_3=29^{\text{th}}$ of October 2021, and $t_4=20^{\text{th}}$ of April 2022.

In Table 3, we discuss in detail the values of the parameters used in equation (2). During the fitting of the mathematical model to the South African data, we divided days according to the number of waves we have. The table compares the transmission rate β, finding the first wave to have a high transmission rate among waves 2 and 3, and this is due to some preventive measures not being implemented. In the presence of vaccination, social distance, and other preventive measures, the fourth wave still tends to have a higher transmission rate compared to all the waves.

The first four plots in Figure 2 can be combined to give the last figure, which depicts the piecewise fitting of the model to the data. What is critical is the initialization of the initial conditions for each wave.

We conceive that the number of infections decreases with increasing social distancing over time. In Figure 3, we vary the efficacy of the social distance parameter when it is 10%, 50%, and 90%. Our result shows that, when the efficacy is between 10% – 50%, it increases the disease infection rate since individuals do not observe the rules of social distancing and COVID-19 transmission mode as seen in Figure 3. The disease persists after a long oscillating transient the infection approaches a positive ω – periodic solution. When the efficacy is 90%, it reduces the infection rate, thereby reducing the transmission rate too.

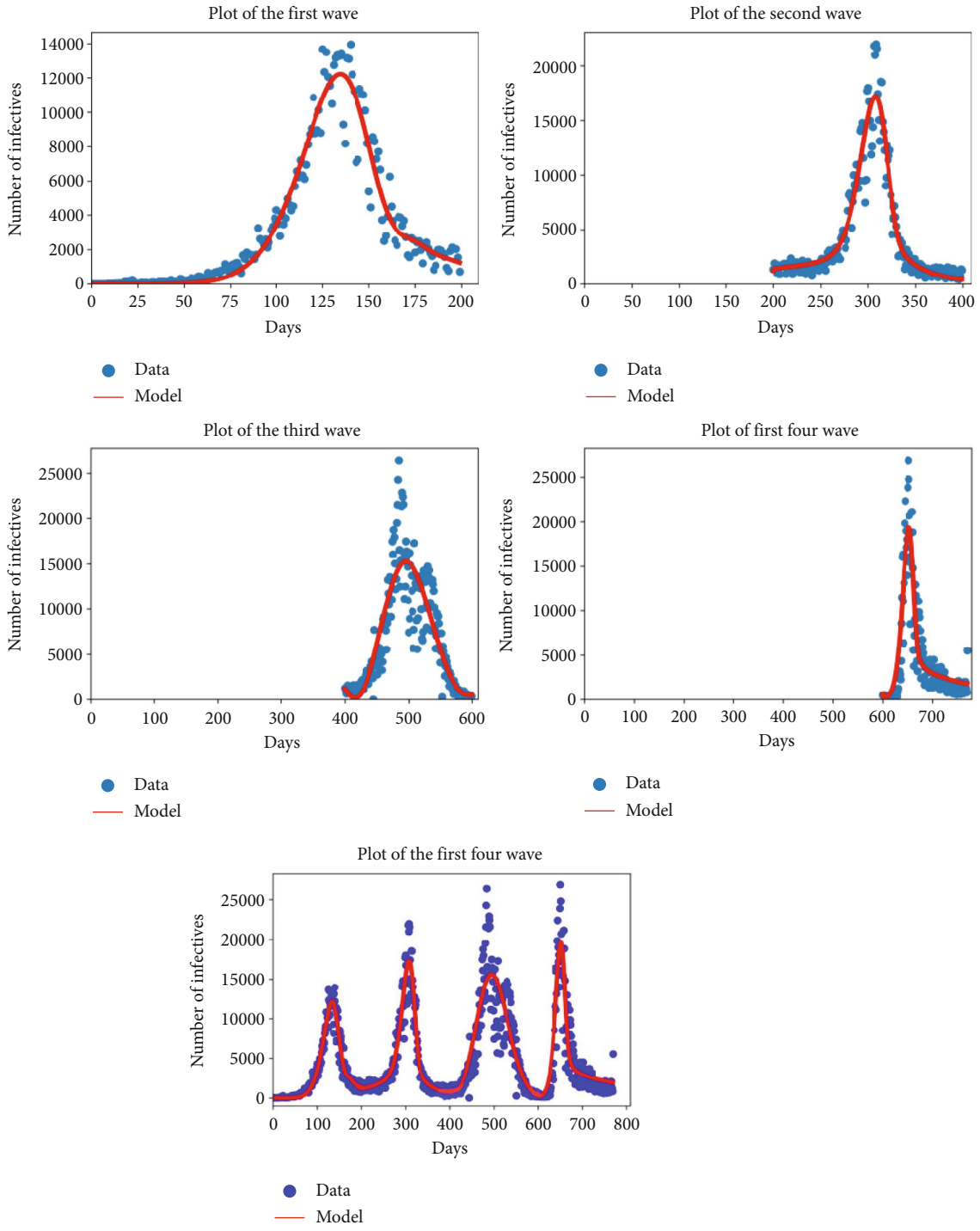

FIGURE 2: New cases in South Africa for the first four waves. The first wave from 27th of March to 11th of September 2020, the second wave from 11th of September 2020 to 10th of April 2021, the third wave from 11th of April to 29th of October 2021, and the fourth wave from 30th of October 2021 to 19th of April, 2022. The blue dots denote the new cases from the data, and the red lines denote our mathematical model prediction. We can see that in each wave, our model constructed fitted well for the given parameters in Table 3.

5. Discussion and Conclusion

We proposed a mathematical model to investigate the coronavirus pandemic in South Africa. We included two unique features in our model: the incorporation of the social distance parameter in the disease transmission dynamics and considering it to be periodic due to climate changes or festive seasons experienced in South Africa. We conducted a detailed analysis of this model and applied it to study the South Africa epidemic using reported data from DSFSI

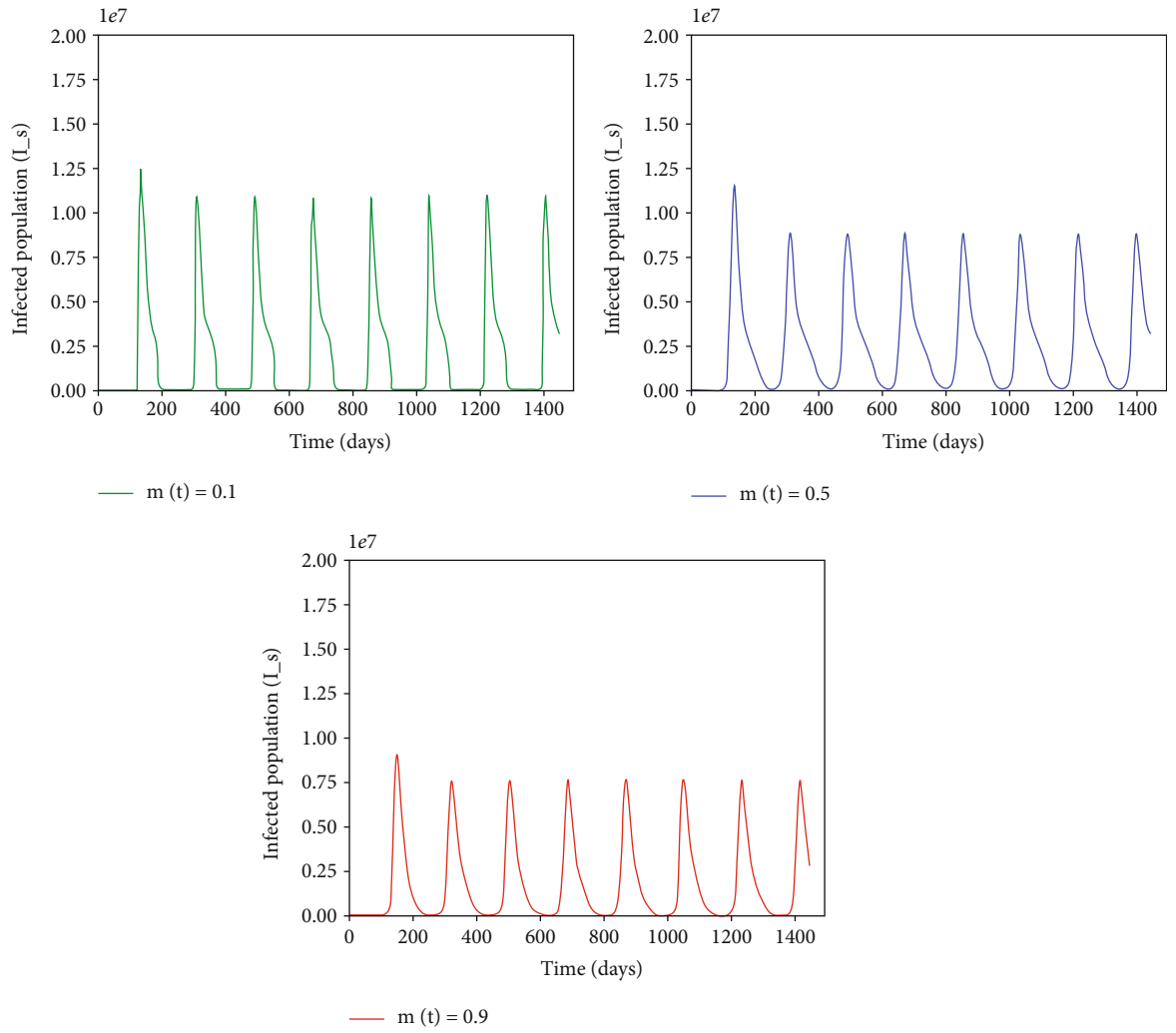

Figure 3: An infection curve of the symptomatic individuals with social distance parameters with efficacies of 10%, 50%, and 90%, respectively; in model 1, parameters are taken from Table 2, the disease persists and a periodic solution with $\omega = 182.5$ days forms after a long transient.

[25]. Our equilibrium analysis of this model shows that the disease dynamics exhibit a threshold at $R_0 = 1$. We have established the global asymptotic stability of the disease-free equilibrium (E^0) when $R_0 < 1$, which implies that the disease dies out, and the global asymptotic stability of the endemic equilibrium (E^1) when $R_0 > 1$, there is at least one positive periodic solution, that is, the disease will spread.

Our numerical simulation results demonstrate the application of our model to COVID-19 in South Africa and the model fit the reported data very well. The numerical simulations also suggest that when raising $\bar{m}$ and $\hat{m}$, respectively, while keeping the other parameters fixed in the transmission rate increases the infection curve. Also, increasing the social distance parameter on a scale of $(0 - 1)$ decreases the infection curve. This means that climate or festive fluctuations should be taken into consideration in designing policies aimed at COVID-19 control and management.

It is widely speculated that COVID-19 would persist and become endemic. From our analysis and numerical simulations, performed over a time interval of 4 years, the disease was still striving and persisting, supporting this speculation. Our results imply that we should be more prepared to fight COVID-19 in the long run beyond this current endemic wave, to reduce the endemic burden and potentially eradicate the disease. We can achieve this when vaccination becomes a requirement.

The model presented in this paper can be improved by incorporating the environmental reservoir into the disease transmission dynamics. When infected individuals cough or sneeze, they spread the virus to the environment through their respiratory droplets which infect other susceptible people with close contact in the same area. The current vaccination drive has the potential of changing the seasonal patterns. However, like influenza, a seasonal vaccination program may be a likely scenario in the case of COVID-19 if it continues to be seasonal. This has the potential of lowering the peaks of the outbreaks and reducing mortality due to the disease.

Data Availability

The data used to support the findings of this study can be accessed through the Coronavirus Data Repository for South Africa 2021 available from https://github.com/dsfsi/covid19za.

Conflicts of Interest

The authors declare there is no conflicts of interest.

Acknowledgments

This study was financially supported by Organization for Women in Science for the Developing World (OWSD), Sida (Swedish International Development Cooperation Agency), and the Department of Mathematics and Applied Mathematics, University of Johannesburg for the production of this paper.

References

[1] Worldometer, "Countries in the world by population," 2022, Technical report. https://www.worldometers.info/world-population/population-by-country/.

[2] R. Li, C. Rivers, Q. Tan, M. B. Murray, E. Toner, and M. Lipsitch, "The demand for inpatient and ICU beds for COVID-19 in the US: lessons from Chinese cities," *MedRxiv*, 2020.

[3] WHO, "World Health Organization: coronavirus disease (COVID-19)," 2019, Technical report. https://www.who.int/health-topics/coronavirus.

[4] C. Bugos, "World Health Organization: coronavirus disease (COVID-19)," 2021, Technical report. https://www.verywellhealth.com/pfizer-developing-covid-19-at-home-treatment-pill-5184029.

[5] M. Diagne, H. Rwezaura, S. Tchoumi, and J. Tchuenche, "A mathematical model of COVID-19 with vaccination and treatment," *Computational and Mathematical Methods in Medicine*, vol. 2021, Article ID 1250129, 16 pages, 2021.

[6] S. Kissler, C. Tedijanto, M. Lipsitch, and Y. H. Grad, "Social distancing strategies for curbing the COVID-19 epidemic," *MedRxiv*, 2020.

[7] L. Matrajt and T. Leung, "Evaluating the effectiveness of social distancing interventions to delay or flatten the epidemic curve of coronavirus disease," *Emerging Infectious Diseases*, vol. 26, no. 8, pp. 1740–1748, 2020.

[8] A. R. Tuite, D. N. Fisman, and A. L. Greer, "Mathematical modelling of COVID-19 transmission and mitigation strategies in the population of Ontario, Canada," *CMAJ*, vol. 192, no. 19, pp. E497–E505, 2020.

[9] R. M. Anderson, H. Heesterbeek, D. Klinkenberg, and T. D. Hollingsworth, "How will country-based mitigation measures influence the course of the COVID-19 epidemic?," *The Lancet*, vol. 395, no. 10228, pp. 931–934, 2020.

[10] G. Makanda, "A mathematical model for the prediction of the impact of coronavirus (COVID-19) and social distancing effect," *WSEAS Transactions on Systems and Control*, vol. 15, pp. 601–612, 2020.

[11] M. J. Keeling, P. Rohani, and B. T. Grenfell, "Seasonally forced disease dynamics explored as switching between attractors," *Physica D: Nonlinear Phenomena*, vol. 148, no. 3-4, pp. 317–335, 2001.

[12] W. P. London and J. A. Yorke, "Recurrent outbreaks of measles, chickenpox and mumps: I. Seasonal variation in contact rates," *American Journal of Epidemiology*, vol. 98, no. 6, pp. 453–468, 1973.

[13] M. E. Martinez, "The calendar of epidemics: seasonal cycles of infectious diseases," *PLoS Pathogens*, vol. 14, no. 11, article e1007327, 2018.

[14] R. Chowdhury, S. Luhar, N. Khan, S. R. Choudhury, I. Matin, and O. H. Franco, "Long-term strategies to control COVID-19 in low and middle-income countries: an options overview of community-based, non-pharmacological interventions," *European Journal of Epidemiology*, vol. 35, no. 8, pp. 743–748, 2020.

[15] Q.-C. Cai, J. Lu, Q.-F. Xu et al., "Influence of meteorological factors and air pollution on the outbreak of severe acute respiratory syndrome," *Public Health*, vol. 121, no. 4, pp. 258–265, 2007.

[16] Z. Huang, J. Huang, Q. Gu, P. Du, H. Liang, and Q. Dong, "Optimal temperature zone for the dispersal of COVID-19," *Science of the Total Environment*, vol. 736, article 139487, 2020.

[17] Z. Bai and Y. Zhou, "Threshold dynamics of a bacillary dysentery model with seasonal fluctuation," *Discrete & Continuous Dynamical Systems-B*, vol. 15, no. 1, pp. 1–14, 2011.

[18] Z. Bai and Y. Zhou, "Global dynamics of an SEIRS epidemic model with periodic vaccination and seasonal contact rate," *Nonlinear Analysis: Real World Applications*, vol. 13, no. 3, pp. 1060–1068, 2012.

[19] NICD, "The national institute for communicable diseases: coronavirus pandemic," 2022, Technical report. https://www.nicd.ac.za.

[20] W. Wang and X.-Q. Zhao, "Threshold dynamics for compartmental epidemic models in periodic environments," *Journal of Dynamics and Differential Equations*, vol. 20, no. 3, pp. 699–717, 2008.

[21] O. Diekmann, M. Gyllenberg, H. Huang, M. Kirkilionis, J. Metz, and H. R. Thieme, "On the formulation and analysis of general deterministic structured population models ii. Nonlinear theory," *Journal of Mathematical Biology*, vol. 43, no. 2, pp. 157–189, 2001.

[22] B. Assan, F. Nyabadza, P. Landi, and C. Hui, "Modeling the transmission of Buruli ulcer in fluctuating environments," *International Journal of Biomathematics*, vol. 10, no. 5, article 1750063, 2017.

[23] V. Lakshmikantham, S. Leela, and A. A. Martynyuk, *Stability Analysis of Nonlinear Systems*, Springer, 1989.

[24] X.-Q. Zhao, *Dynamical Systems in Population Biology, Volume 16*, Springer, 2003.

[25] DSFSI, "Coronavirus data repository for South Africa," 2021, Technical report. https://github.com/dsfsi/covid19za.

[26] Google, "South Africa population," 2021, Technical report. https://www.google.com/search?q=total+population+of+south+africa\&oq=total+pop\&aqs=chrome.2.69i57j0i512l9.6748j0j15\&sourceid=chrome\&ie=UTF-8.

[27] L. Schlein, "Study finds Africa COVID infection grossly underestimated," 2021, Technical report. https://www.voanews.com/a/study-finds-africa-covid-infections-grossly-underestimated/6519320.html.

[28] J. Kleynhans, S. Tempia, N. Wolter et al., "SARS-CoV-2 seroprevalence in a rural and urban household cohort during first and second waves of infections, South Africa, July 2020–March 2021," *Emerging Infectious Diseases*, vol. 27, no. 12, pp. 3020–3029, 2021.